Inertial Laboratory Simulation

C. Blum[1], B. Braun[1], J. Dambeck[1], M. Kägi[2]

[1] Institute of Flight System Dynamics (TUM)
Boltzmannstraße 15
D-85748 Garching bei München
GERMANY

[2] Acutronic Switzerland Ltd
Rosengartenstrasse 25
8608 Bubikon
SWITZERLAND

Abstract

In early 2015 an inertial laboratory will be installed at TUM's Institute of Flight System Dynamics (FSD). In cooperation with ACUTRONIC Switzerland Ltd. an AC3350 three-axis motion simulator will be used to investigate inertial sensor calibration techniques, as well as error influences of the whole laboratory environment. To identify and assess possible influences on the laboratory's quality a simulation of the whole calibration process, including error models of the laboratory environment, the motion simulator and the unit under test has been created. The article presents an overview of identified error sources in the inertial sensor calibration process. Typical error sources are discussed exemplarily for the future Inertial Laboratory. Finally the influence of these errors on a symmetric six-pose calibration process is illustrated using preliminary simulation results.

1. Introduction

The factory calibration of inertial sensors requires a test facility with the ability to apply precisely known motion to the sensor. This is done using a so called motion simulator, which is a kind of industrial robot that is specially designed for a maximum motion accuracy. The motion simulator needs to be placed in a suitable environment, which will be called an inertial laboratory.

Figure 1: ACUTRONIC AC3350 three-axis motion simulator.

From early 2015 on, the Institute of Flight System Dynamics (FSD) of the Technische Universität München and ACUTRONIC Switzerland Ltd., manufacturer of motion simulator systems, will install and operate an inertial laboratory together at Garching, Germany. The three-axis motion simulator AC3350 will be used to investigate inertial sensor calibration procedures, as well as the influences of motion simulator imperfections and external influences on the calibration results. Prior to the installation of the motion simulator, a simulation of the whole chain from the environment, via the foundation and the motion simulator up to the unit under test (UUT) has been created. This allows experimenting on

the influence of different error sources and supports the selection of a proper laboratory location as well as the dimensioning of a floating foundation.

While there are many publications about the calibration of inertial sensors, there are only few publications that focus on the influences of the inertial laboratory. Usually only imperfections of the motion simulator are investigated (e.g. [1], [2]). In addition to the sensor's and motion simulator's errors, the created simulation also includes the coupling to the environment and thus allows the investigation of external disturbances as well as dynamic effects caused by the oscillatory excitation of the foundation.

The Institute of Flight System Dynamics has access to a wide range of sensor classes, ranging from low-cost consumer-grade units, over tactical grade IMUs like the NGL µIMU up to navigation grade RLG sensors used in the iMAR iNAV-RQH. This supports the validation of the simulation model for additional test cases.

2. Environmental influences

The word laboratory implies a controlled environment in which the desired experiments can be conducted. As an inertial laboratory is meant to generate precisely known motions, the transfer of unwanted motions from the environment to the motion simulator needs to be investigated. Where the motion simulator is linked to the ground, motions of the surface are transferred to the turntable and consequently to the unit under test.

Motions of the Earth's surface are usually described as surface waves. These waves can be caused by seismic activities, like earthquakes, as well as being human made. Any oscillating machine (including vehicles) which is placed on the ground emits surface waves. Among the different types of surface waves, the so called Rayleigh-Waves have the highest amplitudes and are therefore most critical for vibration protection. These waves create longitudinal and transversal oscillations of a characteristic ratio, which changes with the depth below ground.

Before installing an Inertial Laboratory, the planned location has to be examined for potentially disturbing surface-wave sources. An overview of the future laboratory location at the campus Garching is presented in Figure 2. Four major sources of surface waves have been identified:

- road (A) at a distance of 40m,
- subway (B) at a distance of 250m,

- wind tunnel (C) at a distance of 50m,
- unspecified machinery (D), distributed over the area

While literature values for the surface-wave emissions from subways and roads are available, the influence of a wind tunnel and the various unknown machinery at the campus cannot be determined yet.

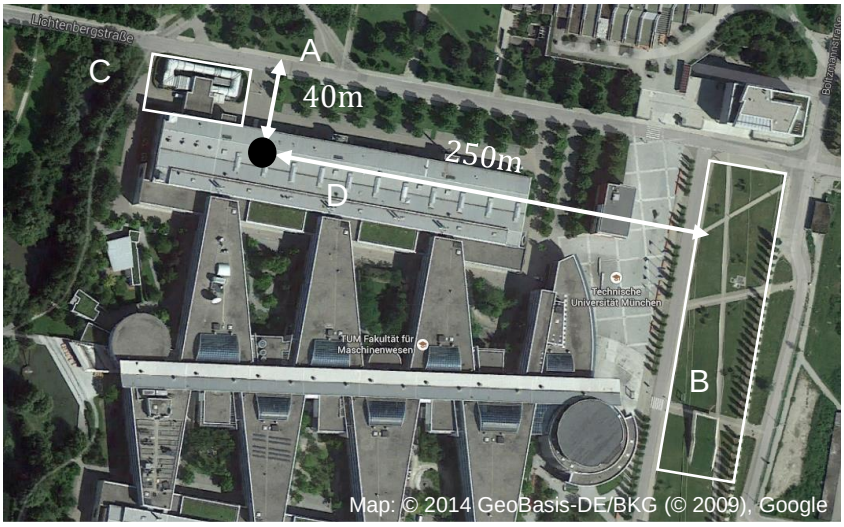

Figure 2: Surface wave sources at future laboratory location.

According to [3] the amplitude reduction of Rayleigh-Waves with the distance can be approximated as:

$$U = U_0 \left(\frac{r}{r_0}\right)^{-1.1} \tag{1}$$

Applying this formula the literature amplitude values of $U_{0,truck} = 0.04\,\frac{mm}{s}$ and $U_{0,subway} = 0.3\,\frac{mm}{s}$ returns a remaining amplitude of $U \approx 6.9 \cdot 10^{-4}\,\frac{mm}{s}$ at the laboratory location for both sources. In the next section, we will demonstrate that the truck's emissions at $f = 5\ to\ 15$ Hz lie nearer to the foundation's natural frequency than the subway's emissions of $f = 40\ to\ 60$ Hz. Thus, the road can be considered as the most important environmental disturbance source.

3. Laboratory setup

To limit disturbances from the laboratory building, it is recommended to mount the motion simulator on a floating foundation. This floating foundation is modelled using a classical machine-bed design approach by the *Committee on "Soil Dynamics" of the German Geotechnical Society* [4].

As illustrated in Figure 3, the interaction between the foundation and the soil is modeled as a set of spring-damper elements for each degree of freedom. Each of the six elements attacks the foundation at the bottom, below its center of gravity.

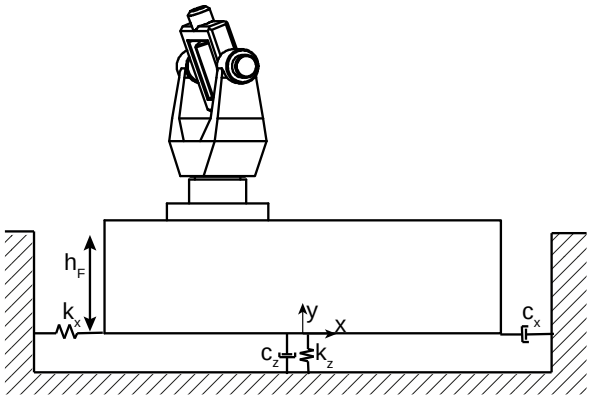

Figure 3: Model of foundation and soil interaction.

In [4] a set of formulas that relate spring- and damping constants for each degree of freedom to the soil's dynamic shear modulus G_d, density ρ_s and Poisson's ratio ν as well as to the foundation's dimensions, is presented. While the Poisson's ratio has little influence, the shear modulus is directly related to the spring's stiffness and therefore to the natural frequency of the foundation/soil system in each respective degree of freedom.

Soft soil leads to low natural frequencies, which is desirable for an amplitude reduction of surface waves on the one hand, but allows high amplitudes for direct excitation on the other hand. A high damping ratio is desirable, as it provides a fast declining of excitations. As the soil of a planned location usually cannot be changed, the desired decoupling must be set by dimensioning of the foundation and, if necessary, additional damping-elements between foundation and soil.

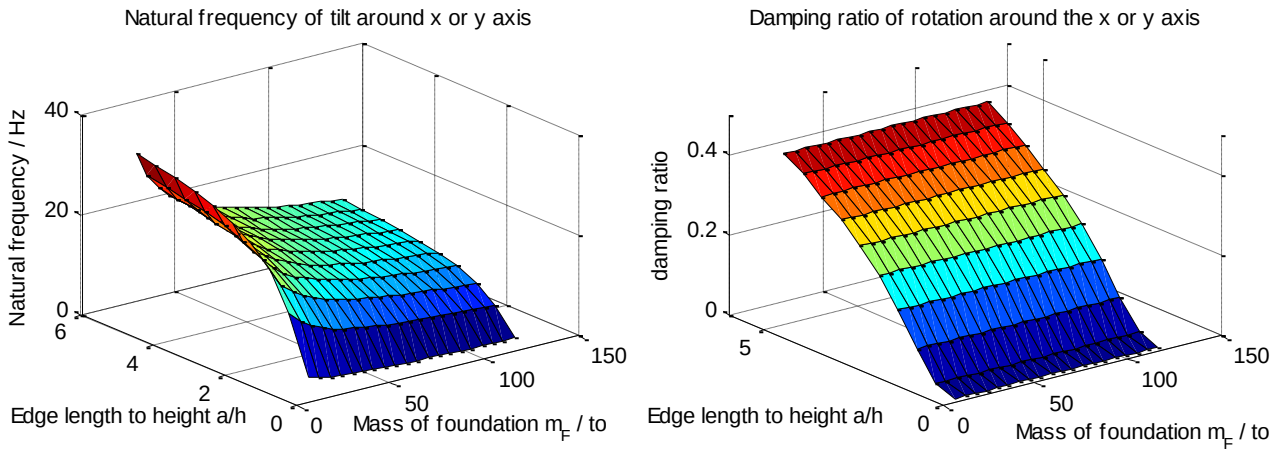

Figure 4: Influence of foundation dimensions on oscillation characteristics.

The influence of foundation geometry on the oscillation properties of a quadratic foundation is illustrated in Figure 4. The displayed shape of the curves can be observed for all other degrees of freedom, too. The planned foundation for our AC3350 motion simulator will have natural frequencies of $10 - 20\ \mathrm{Hz}$, depending on the true stiffness of the soil. While the natural frequency declines with growing foundation mass, the damping ratio is nearly unaffected. The demands for a low natural frequency and a large damping ratio introduce opposing requirements to the foundation's dimensions: A sleek, pile-like foundation lowers the natural frequency while a high damping requires a wide, expanding foundation. To design a foundation to a desired natural frequency and damping, the future location had to be examined for soil parameters as well as for the frequencies of existing disturbances.

In section 2, the road near the laboratory was identified as the most important source of surface waves. The introduced spring-damper model is now used to estimate the motion that is generated by a passing truck on this road. The simulated setup for the future laboratory is summarized in Table 1.

Table 1: Simulated test case.

Foundation dimensions	$4.5\mathrm{m} \times 3.5\mathrm{m} \times 2\mathrm{m}$, not embedded
Soil parameters	$G_d = 10\mathrm{MPa}$, $\nu = 0.3$, $\rho = 1900\ kg/m^3$ (estimated)
Motion Simulator	ACUTRONIC AC3350
	Positioned $\Delta x = 1.5\mathrm{m}$, $\Delta y = 1.0\mathrm{m}$ from found. center
Alignment	local levelled ENU-frame
Location	48°16'00.3"N 11°40'07.2"E, 476m
Gravity	$g = 9.80745\ \mathrm{m/s^2}$, no deflection considered

The truck has an assumed velocity of $v = 36\ km/h$ and emits harmonic oscillations with an amplitude $U_0 = 0.04 \frac{mm}{s}$ at $f = 10\text{Hz}$. The resulting angular rates and accelerations at the UUT's position that are caused by this excitation are presented in Figure 5.

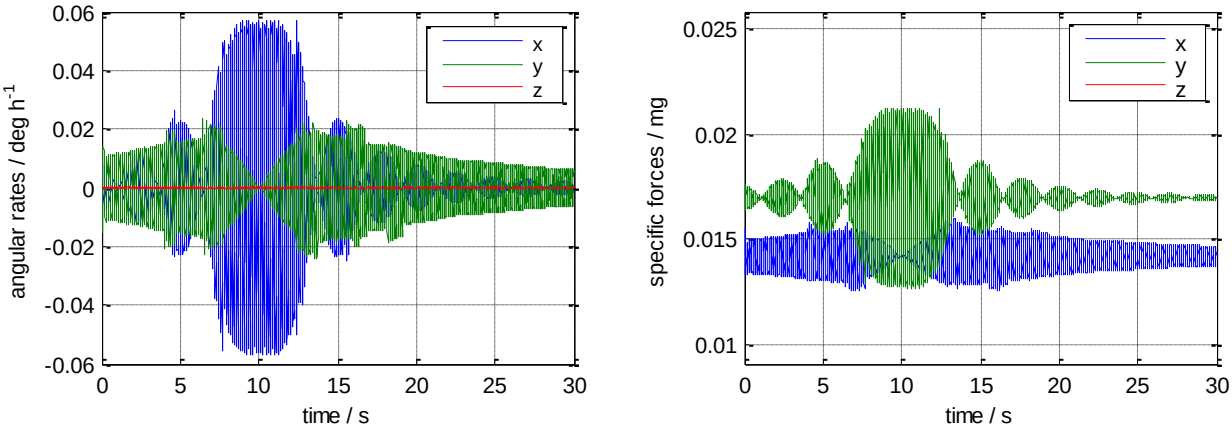

Figure 5: Resulting UUT motion caused by a passing truck.

Figure 5 indicates that the foundation is excited to angular rate amplitudes of $0.06\ °/\text{h}$. The resulting acceleration at the UUT's position sums up to 0.05mg. The influence of such a disturbance on the calibration results strongly depends on the sensor class as well as on the calibration procedure, and cannot be generally assessed yet.

As mentioned before, a soft soil allows high amplitudes for direct excitation. Direct excitations are either caused by external forces or by reaction forces from the motion simulator. To counter these forces with the maximum inertia of the foundation, ACUTRONIC recommends the motion simulator to be placed acentric on the foundation.

As a vivid example of how direct dynamic loads excite the foundation we simulated a walking person on the foundation, which is only a theoretical consideration for safety reasons. The person is assumed to walk along the long edge of the foundation. The thereby attacking forces are determined from a civil-engineering model of the human walk that is used to analyse resonance effects of pedestrian bridges. The model assumes an average human weight of $G = 800\text{N}$ and a step frequency of $f = 2.2\text{Hz}$.

The resulting angular rates and accelerations at the UUT's position, due to this excitation, are presented in Figure 6. Compared to the results of the truck simulation, the amplitudes are two magnitudes higher. Though the influence of these disturbances on calibration results still cannot be generally assessed, the large amplitudes indicate a major influence.

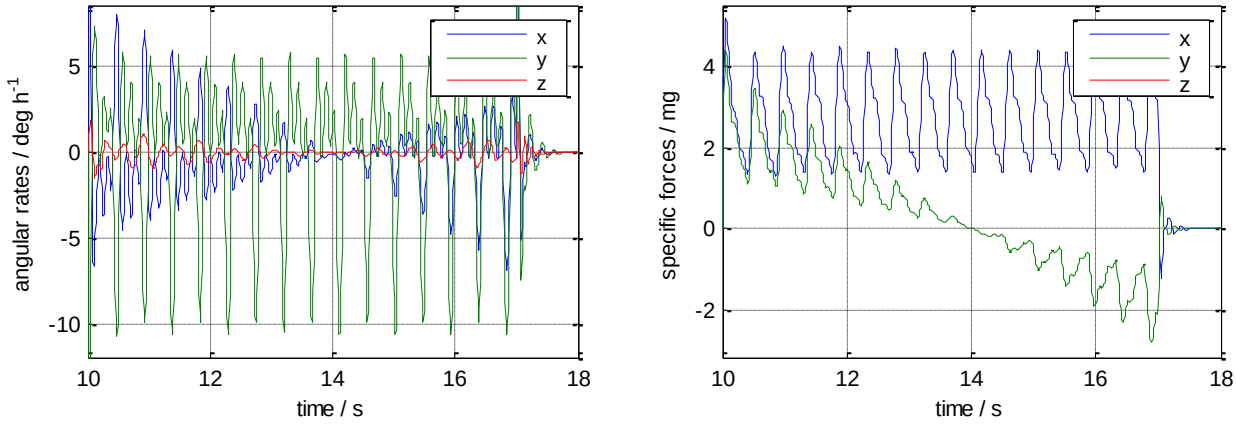

Figure 6: Resulting UUT motion caused by a walking human.

In addition to external forces the foundation can also be excited by centrifugal forces. These occur, if the centre of gravity of the UUT and its mounting adapter does not lie on the rotation axis. In this case the centrifugal force rotates with the respective gimbal and therefore excites the foundation to an oscillating motion. The foundation's tilt follows the gimbal's position with a phase delay, depending on the angular rate of the gimbal.

The AC3350 motion simulator provides a free space of $0.4\mathrm{m} \times 0.4\mathrm{m}$ at the inner gimbal and allows a maximum payload of $16\mathrm{kg}$. As a worst case scenario, a $16\mathrm{kg}$ UUT is mounted with $0.2\mathrm{m}$ offset to the rotation axis and rotated at a rate of $400\,°/s$. The motion of the UUT position that is caused by the foundation's motion is presented in Figure 7.

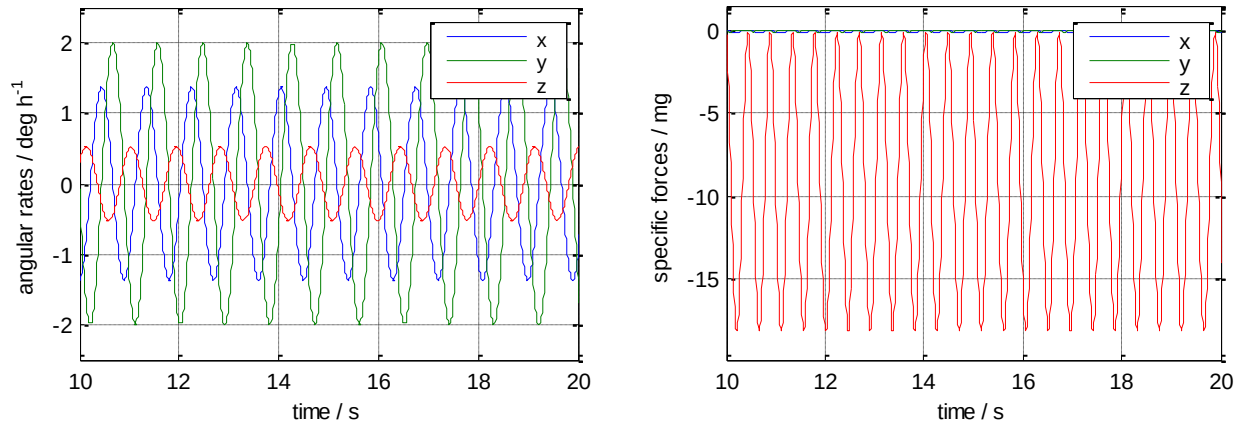

Figure 7: Resulting UUT motion caused by centrifugal forces.

The resulting amplitudes are of the same magnitude as the results for the walking human test case. This emphasizes the necessity to balance each gimbal around the rotation axis properly.

4. Laboratory surveying

As stated before, a laboratory should provide a known environment. In addition to a suitable decoupling from environmental disturbances, this requires the knowledge of the local orientation of the Earth's angular rate and the local gravity vector. The orientation of both vectors directly depends on the leveling and orientation of the motion simulator. The leveling is usually conducted using a precision spirit level or a digital inclinometer, which allow an accuracy of ≈ 1" respectively ≈ 0.1".

North orientation can be accomplished by targeting reference points (e.g. landmarks) or by performing a stationary alignment using a navigation grade IMU. While north orientation is critical for the installation of a 2-axis motion simulator, it is just an arbitrary origin that can be adjusted in software for a 3-axis simulator. In addition to the alignment, the geodetic latitude of the laboratory influences the orientation of Earth's angular rate. For the future laboratory location the angular rates' orientation error due to a position error is approximately $^{1}/_{1000}\,^{\circ}$ per $110\mathrm{m}$.

In contrast to the Earth's angular rate, both magnitude and direction of the local gravity vector depend on the laboratory's position. Besides an expensive gravimetrical examination of the location, the local gravity can also be determined from models and databases. The DSHN96 is a Germany-wide database of gravimetrical measurements that allows interpolation of gravimetrical data for any point in Germany. Gravity magnitude values with an accuracy better than $10\mathrm{ppm}$ can be accessed on the website of the *Bundesamt für Kartographie und Geodäsie* [5]. In contrast to the DHSN96, the Earth Gravity Model 2008 (EGM2008) is a spherical harmonics model for the whole planet based on satellite measurements and allows the determination of the gravity vector including deflections from the reference ellipsoid. As the EGM2008 has only a spatial resolution of $9.3\mathrm{km}$ [6], usual positioning errors may be neglected for its use. Using Somigliana's gravity formula with free air reduction [7], the change of gravity magnitude with the altitude for the laboratory's location can be estimated as:

$$\frac{\partial \gamma}{\partial h} = -3.14 \cdot 10^{-4} \frac{\mathrm{mg}}{\mathrm{m}} \tag{2}$$

Note that typical leveling devices use local gravity as a reference. The motion simulator is therefore not aligned to the ideal local level frame of the reference ellipsoid, but to the local gravity vector. Usually these deflections are less than 20", but may raise up to 120" in alpine

regions. For our laboratory location the EGM2008 predicts a meridional deflection of $\xi = -2.70"$ and a deflection from the prime vertical of $\eta = -0.97"$.

5. Motion simulator

In an inertial laboratory motion simulators (“turntables”) are used to apply a precisely known motion to the tested inertial instrument. Therefore, they have a major impact on the laboratory’s overall quality.

As displayed in Figure 8, the three-axis motion simulator AC3350 can be represented by a multi-body model of six rigid bodies.

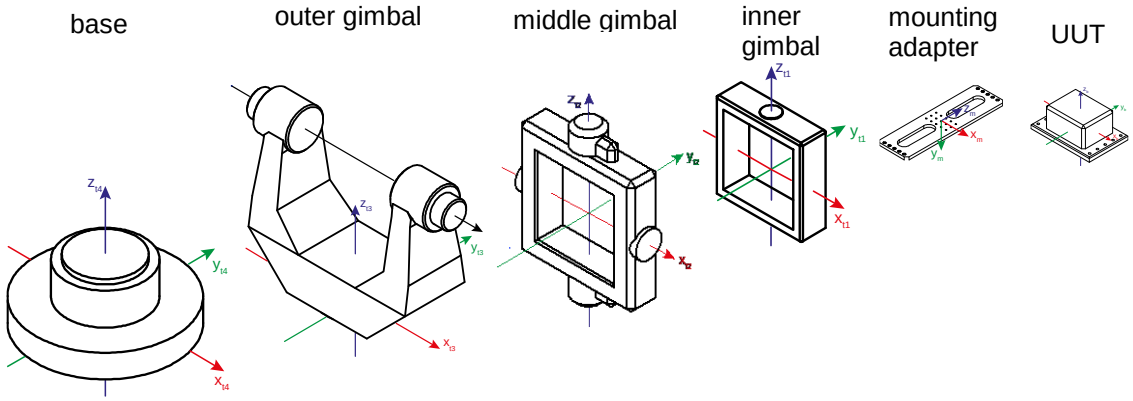

Figure 8: Three axis motion simulator multi-body model.

The motion simulator itself consists of a base-element, and three gimbals that are placed within each other. While the outer gimbal rotates around the vertical axis, the middle gimbal rotates around the horizontal axis that is fixed to the outer gimbal. The inner gimbal however rotates around the vertical axis that is fixed to the middle gimbal. The UUT is connected to the inner gimbal using a mounting plate. Their position and orientation are constant with respect to the inner gimbal.

Assuming an ideal motion simulator, without any imperfections and environmental disturbances, the angular rate of the UUT can be composed from the Earth’s angular rate ω_{ie}, the angular positions α, β, γ and associated rates of the three gimbals (equation (3)). The angular positions, rates and accelerations are commanded by the operator. For an ideal motion simulator the base is assumed to be aligned to the local levelled ENU-frame. Using the positions, rates and angular accelerations together with the local gravity vector (see section 4.) allows the determination of the UUT’s specific forces (equation (4)).

$$\boldsymbol{\omega}_{ib} = \mathbf{R}_{bt_1}\left(\begin{bmatrix}0\\0\\\dot{\alpha}\end{bmatrix} + \mathbf{R}_{t_1t_2}(\alpha)\left(\begin{bmatrix}\dot{\beta}\\0\\0\end{bmatrix} + \mathbf{R}_{t_2t_3}(\beta)\left(\begin{bmatrix}0\\0\\\dot{\gamma}\end{bmatrix} + \mathbf{R}_{t_3l}(\gamma)\,\mathbf{R}_{le}(\phi)\,\boldsymbol{\omega}_{ie}\right)\right)\right) \quad (3)$$

$$\boldsymbol{f}_b = \mathbf{R}_{bt_1}\left(\boldsymbol{\Omega}_{it_1}\boldsymbol{\Omega}_{it_1}\,\boldsymbol{r}_{t_1}(G_{UUT}) + \dot{\boldsymbol{\Omega}}_{it_1}\boldsymbol{r}_{t_1}(G_{UUT}) - \mathbf{R}_{t_1t_2}(\alpha)\,\mathbf{R}_{t_2t_3}(\beta)\,\mathbf{R}_{t_3l}(\gamma)\,\boldsymbol{\gamma}_l\right) \quad (4)$$

with

$\mathbf{R}_{le}(\phi)$	Transformation matrix from ECEF to ENU frame
$\mathbf{R}_{t_3l}(\gamma)$	Transformation matrix from ENU to outer gimbal frame
$\mathbf{R}_{t_2t_3}(\beta)$	Transformation matrix from outer gimbal to middle gimbal frame
$\mathbf{R}_{t_1t_2}$	Transformation matrix from middle gimbal to inner gimbal frame
$\mathbf{R}_{bt_1}$	Transformation matrix from inner gimbal to UUT body-fixed frame
$\boldsymbol{r}_{t_1}(G_{UUT})$	Position of the UUT's centre of gravity, represented in the inner gimbal frame
$\boldsymbol{\gamma}_l$	Local gravity vector, represented in local levelled ENU-frame
$\boldsymbol{\omega}_{ie}$	Earth's angular rate, represented in ECEF-frame
$a, \dot{a}, \ddot{a}$	Angular position, rate and acceleration of the inner gimbals rotation axis
$\beta, \dot{\beta}, \ddot{\beta}$	Angular position, rate and acceleration of the middle gimbals rotation axis
$\gamma, \dot{\gamma}, \ddot{\gamma}$	Angular position, rate and acceleration of the outer gimbals rotation axis
$\boldsymbol{\Omega}_{it_1}$, $\dot{\boldsymbol{\Omega}}_{it_1}$	Skew symmetric matrix of the angular rate / acceleration of the inner gimbal towards the inertial frame

The UUT's motion is not only corrupted by the external influences, which were discussed before, but also the motion simulator itself contains imperfections that lead to an erroneous motion. Typical motion simulator errors that are specified by the manufacturer include: axis non-orthogonality, wobble, position accuracy and rate stability.

As illustrated in Figure 9a axis non-orthogonality means that the rotation axes are not perfectly orthogonal to each other. In addition to this static orientation error, the axes perform a tilting motion depending on the gimbals angular position, called wobble. The rotation axis moves on the surface of a distorted cone, which is illustrated in Figure 9b. The orientation error caused by these imperfections are typically less than 5".

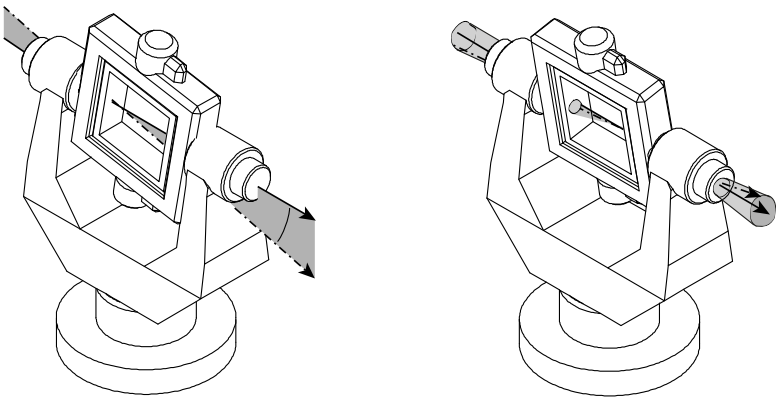

a) non-orthogonality b) wobble

Figure 9: Motion simulator imperfections.

While the previous two errors are caused by hardware-imperfections, the achievable position accuracy is influenced by the resolver's accuracy as well as by the used controller. Typical positioning errors are less than $5"$. The same factors influence the rate-stability, which is a measure of how well a desired angular rate is kept. Typically the average angular rate over one full turn differs less than $2\mathrm{ppm}$ from the desired rate.

During dynamic operation additional influences like mechanical stiffness and vibrations may occur, but are not considered in the simulation yet.

6. Unit Under Test

The aim of an inertial sensor calibration is to identify and determine deterministic errors of the sensor's output. IEEE Std. 647 [8] proposes the following model equations for bias-like errors to be used for inertial sensor simulation:

$$(\mathbf{I}+\mathbf{S}_\omega)\tilde{\boldsymbol{\omega}}_{ib}(t)+\boldsymbol{f}\big(\boldsymbol{\omega}_{ib}(t)\big)=\boldsymbol{\omega}_{ib}(t)+\mathbf{M}_\omega\boldsymbol{\omega}_{ib}(t)+\mathbf{A}_\omega\boldsymbol{f}_b(t)+\boldsymbol{b}_\omega(t) \tag{5}$$

$$\big(\mathbf{I}+\mathbf{S}_f\big)\tilde{\boldsymbol{f}}_b(t)+\boldsymbol{f}\big(\boldsymbol{f}_b(t)\big)=\boldsymbol{f}_b(t)+\mathbf{M}_f\boldsymbol{f}_b(t)+\boldsymbol{b}_f(t) \tag{6}$$

These equations include:

- scale factor errors $\mathbf{S}$,
- axis misalignment $\mathbf{M}$,
- bias terms $\boldsymbol{b}(\boldsymbol{t})$ and
- acceleration dependant errors $\mathbf{A}_\omega$ (gyro only).

For a first analysis, we used a simplified error model, neglecting acceleration dependency of the gyro and assuming a constant bias (see equation (7), (8)).

$$\tilde{\boldsymbol{\omega}}_{ib}=\begin{bmatrix}b_{\omega,x}\\b_{\omega,y}\\b_{\omega,z}\end{bmatrix}+\left(\begin{bmatrix}0&M_{\omega,xy}&M_{\omega,xz}\\M_{\omega,yx}&0&M_{\omega,yz}\\M_{\omega,zx}&M_{\omega,zy}&0\end{bmatrix}+\begin{bmatrix}S_{\omega,x}&0&0\\0&S_{\omega,y}&0\\0&0&S_{\omega,z}\end{bmatrix}\right)\boldsymbol{\omega}_{ib}+\boldsymbol{\nu}_\omega \tag{7}$$

$$\tilde{\boldsymbol{f}}_b = \begin{bmatrix} b_{f,x} \\ b_{f,y} \\ b_{f,z} \end{bmatrix} + \left(\begin{bmatrix} 0 & M_{f,xy} & M_{f,xz} \\ M_{f,yx} & 0 & M_{f,yz} \\ M_{f,zx} & M_{f,zy} & 0 \end{bmatrix} + \begin{bmatrix} S_{f,x} & 0 & 0 \\ 0 & S_{f,y} & 0 \\ 0 & 0 & S_{f,z} \end{bmatrix} \right) \boldsymbol{f}_b + \boldsymbol{\nu}_f \tag{8}$$

To consider the influence of sensor noise on the calibration process, a noise term $\boldsymbol{\nu}$ is added. This noise is synthesized from typical inertial sensor noise effects. A sample Allan-deviation plot, illustrating the amplitudes and frequency ranges of the different effects, is presented in Figure 10.

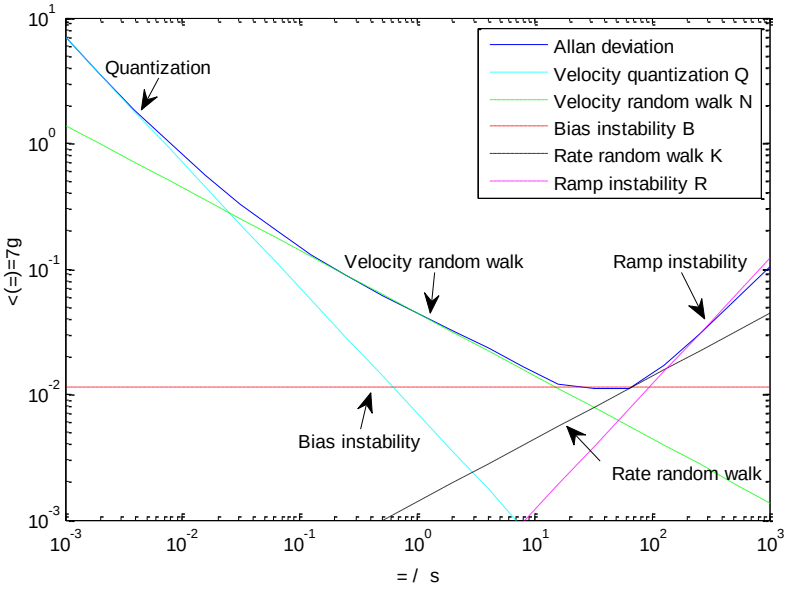

Figure 10: Synthesis of an accelerometer noise model.

The simplified error model contains 12 unknowns for each sensor that can be identified using at least four poses of static orientation respectively angular rates.

7. Preliminary simulation results

During a calibration procedure the deterministic IMU errors are estimated using the theoretical motion, which is determined from the motion simulator's output. To determine the IMU errors using this estimated motion, the errors between the actual and the estimated motion must be less than the investigated IMU errors.

To investigate the influence of the previously described laboratory errors on a typical calibration, a six-pose symmetric gyro calibration is simulated with angular rates of $40°/s$ and using the averaged data of $90s$ per pose. To focus on the laboratory's influence only, the inertial sensor is assumed to have just bias-like errors and neither noise nor limited resolution. The here presented results are preliminary. They are only intended to illustrate the kind of results that is expected from future investigations. The influence on bias-like error estimates is determined by subtracting the calibration results determined from true motion

from the results determined from estimated motion. The resulting absolute values of the errors are presented in Figure 11. The following test cases have been simulated:

- Controller/resolver: Position and rate inaccuracy.
- UUT positioning: $1\mathrm{kg}$ UUT placed $0.1\mathrm{m}$ in x_{t1}-direction from rotation axis.
- Wobble: wobble model, from measurements, $0.27"$ average tilt.
- Non-orthogonality: $5"$ non-orthogonality between each two rotation axis.
- Non-orthogonality and wobble together.

The general laboratory setup equals the setup described in Table 1.

While the resulting errors for the scale factor estimation are far below typical navigation grade specifications for any test case, the results for the bias and especially misalignment estimation do not achieve those navigation grade specifications. This indicates that the simulated 6-rate-pose calibration is sufficient for scale factor determination and possibly for bias estimation. The misalignment estimation however, should be performed using a more sophisticated calibration profile that compensates the motion simulator's axis orientation errors.

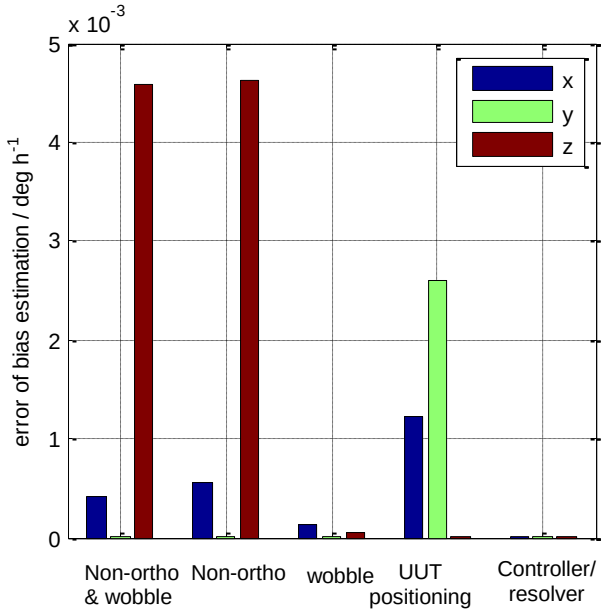

a) error of bias estimation

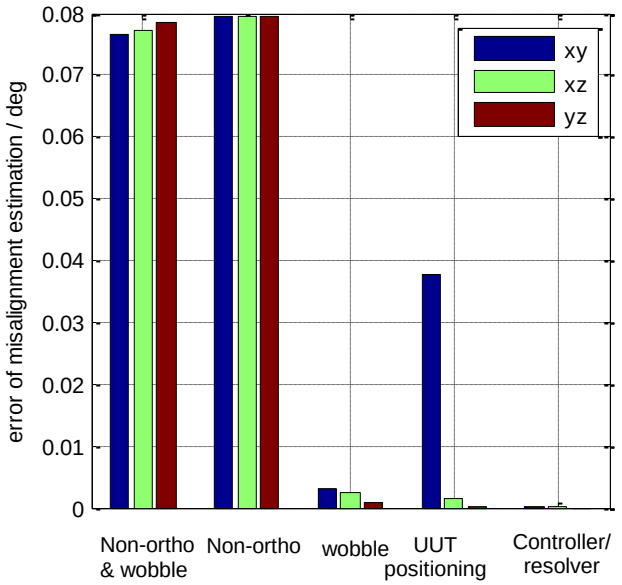

b) error of misalignment estimation

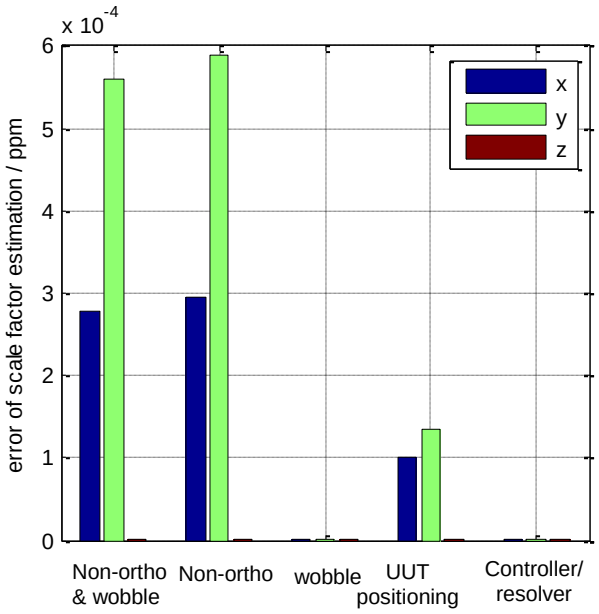

c) error of scale factor estimation

Figure 11: Influence of motion simulator errors on 6-pose gyro calibration results.

The simulation of combined non-orthogonality and wobble illustrates that the effect of this combination is not just the sum of the single effects of wobble and non-orthogonality.

The high estimation errors due to an acentric positioning of the UUT emphasize the necessity to balance each gimbal around the rotation axes properly.

Though these preliminary results do not allow a general statement on the achievable calibration accuracy yet, they strengthen the need for a detailed analysis of the whole calibration chain, at least for navigation grade sensors.

8. Conclusion and outlook

The preliminary results, presented in section 7, indicate that the used forward-simulation approach is suitable to examine error influences on the inertial instrument calibration process. Typical errors, caused by the environment, handling errors and motion simulator imperfections have been presented and discussed. Though a universal statement on their influence on a calibration process cannot be presented yet, the importance of a proper consideration of these errors is illustrated.

After the installation of the inertial laboratory at FSD, the simulation results will be validated and generalized to form recommendations for inertial laboratory setup and operation. In addition, future research will include monitoring and compensation of laboratory's errors as well as the design of profiles for an effective sensor calibration.

References

[1] G. Wei, F. Xirui und L. Fengli, „Analysis on the Influence of Three-axis Turntable Nonorthogonal Error on Gyro Calibration of SINS,“ in *Proceedings of 2012 IEEE International Conference on Mechatronics and Automation*, Chengdu, 2012.

[2] N. Andrianos, C. Diez und L. DeMore, „Flight table orientation error transparency for hardware-in-the-loop facilities,“ in *Proc. SPIE 4366 Technologies for Synthetic Environments: Hardware-in-the-Loop Testing VI*.

[3] H. Kramer, Angewandte Baudynamik, Berlin: Ernst & Sohn, 2013.

[4] Empfehlungen des Arbeitskreises "Baugrunddynamik" der Deutschen Gesellschaft für Geotechnik e.V., Berlin: Grundbauinst. der Techn. Univ. Berlin, 1998.

[5] Bundesamt für Kartographie und Geodäsie, "Onlineberechnung des Schwerewertes," [Online]. Available: http://www.bkg.bund.de/nn_175464/DE/Bundesamt/Geodaesie/GeodIS-WA/WApp/SwrBer/swrber00__node.html__nnn=true. [Accessed 08 09 2014].

[6] N. Pavlis, S. Holmes, S. Kenyon and J. Factor, "The development and evaluation of the Earth Gravitational Model 2008 (EGM2008)," *Journal of Geophysical Research: Solid Earth,* 2012.

[7] Department of Defense World Geodetic System 1984, 3rd ed ed., vol. NIMA TR8350.2, Bethesda, Md.: National Imagery and Mapping Agency, 1997.

[8] *IEEE Standard Specification Format Guide and Test Procedure for Single-Axis Laser Gyros,* 2006.